Classical chaos and ballistic transport in a mesoscopic channel

G. A. Luna-Acosta

Ilya Prigogine Center for Studies in Statistical Mechanics and Complex Systems, University of Texas, Austin, Texas 78712-1081
and Instituto de Física, ''Luis Rivera Terrazas,'' Universidad Autónoma de Puebla, Apartado Postal J-48, Puebla 72570, Mexico

A. A. Krokhin, M. A. Rodríguez, and P. H. Hernández-Tejeda

Instituto de Física, ''Luis Rivera Terrazas,'' Universidad Autónoma de Puebla, Apartado Postal J-48, Puebla 72570, Mexico
(Received 6 September 1995; revised manuscript received 5 February 1996)

We study transport properties in the classical ballistic regime of a two-dimensional electron channel with sinusoideal (rippled) boundaries. We calculate the transmission coefficient, the average number of collisions, and the mean path length, as a function of ripple amplitude. The Poincaré plots of the associated dynamical system (the infinitely long channel) exhibit the generic transition to chaos as the amplitude of the ripples is increased. The chaotic nature of the finite channel is manifested by the fractal character of a response function. Transport features and dynamical properties are correlated. We compare our results with those that consider collisions with random (rough) boundaries. A criterion is proposed to distinguish between regular and chaotic dynamics by measuring classical resistivity. [S0163-1829(96)02240-0]

I. INTRODUCTION

The development of nanostructure technology and the advances in the theory of dynamical systems has led to the search for signatures of chaos in the transport properties of mesoscopic samples. Important results have recently been obtained in quantum transport, i.e., in phenomena where the wave nature of electrons plays a fundamental role. For example, measurements of magnetoresistance in ballistic microstructures in the shape of a ''chaotic'' billiard and the circle showed clear distinctions in the power spectrum of universal conductance fluctuations and in the line shape of the weak localization peak.[1,2] This line of investigation pertains to the very prolific field of quantum chaos, the study of the quantum manifestations of classical chaos.[3] In this paper, however, we address another important aspect, namely, the search for signatures of chaos in classical transport properties. The classical counterpart of universal quantum fluctuations of conductance has been studied in Refs. 4 and 5. Classical resistivity of ballistic cavities with either regular or chaotic dynamics of electrons was analyzed in Ref. 6, where it was shown that dynamical chaos is responsible for the well-known additive property for resistors connected in series. Within the framework of the classical billiard-ball model,[7] various effects in narrow electronic channels can be understood if the number of transverse channels is large enough (even 3 may be sufficient).[8–12]

The present work is concerned with classical ballistic transport through a two-dimensional channel formed between a sinusoidal (rippled) and a flat boundary (see Fig. 1). Certain features of the quantum-classical correspondence of this system have been studied in Ref. 13. The trajectories are deterministic but not integrable, hence there is regular and chaotic scattering at the boundaries. As the amplitude of the ripple is increased the electron dynamics changes from regular to mixed and to global chaos. Transport characteristics of the channel that can be measured experimentally, e.g., resistivity, depend on these distinct dynamical regimes. We cor-

relate the transport properties of the finite channel with the dynamical properties of the infinite channel. Based on this, we obtain a criterion that allows a distinction between regular and chaotic motion by measuring the classical resistivity of the channel.

II. CLASSICAL TRANSPORT PROPERTIES

Figure 1 specifies the geometry of the channel. The top profile is given by $Y = d + a\sin(2\pi X/b)$. L is the length of the channel. It is convenient to write the profile in dimensionless coordinates as $y \equiv Y/b = \gamma + \nu\sin(2\pi x)$, where $x \equiv X/b$, $\nu \equiv a/b$, $\gamma \equiv d/b$, and $l \equiv L/b$. Assuming the simplest con-
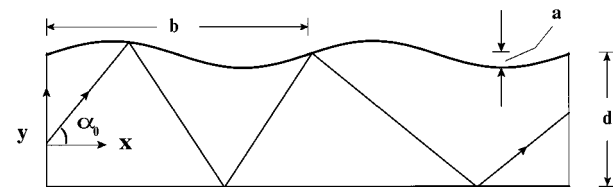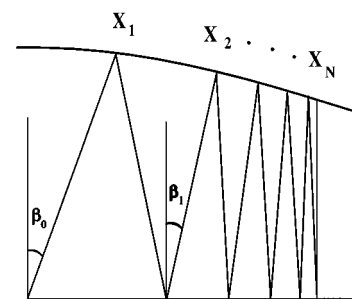
FIG. 1. Geometry of the rippled channel and real-space trajectories of an electron (a) transmitted to the right and (b) executing librational motion in adiabatic regime.

nection to the lead, the initial distribution is given by

$$\rho(\alpha_0) = (n_0/2d)\cos\alpha_0, \qquad (1)$$

where α_0 is the angle of incidence [see Fig. 1(a)] and n_0 is the number of electrons (typically 10^5) injected on the left-hand side.

The trajectory of each electron (all with the same magnitude of velocity) defined by its initial condition (y_0, α_0) is followed, keeping a record of the number of collisions with the boundaries and the length it travels before it leaves the channel to the right or to the left. The transmissivity T, the mean number of collisions for transmitted particles $\langle N_t \rangle$, and the mean path length $\langle \lambda_t \rangle$ are computed for a given set of geometrical parameters (ν, γ, l). $\langle \lambda_t \rangle$ ($\langle N_t \rangle$) is the total path length (sum of all collisions) of all the transmitted particles divided by the number of transmitted particles. Transmissivity is the flux of transmitted particles divided by the incoming flux.

Consider a channel with few periods of ripples. We shall look at two prototypical shapes. The combination $\gamma = 5$ and $l = 2$ produces a short and wide channel, i.e., its length is 2/5 its width. For brevity we shall refer to it as a SW channel. The combination $\gamma = 0.1$ and $l = 2$ produces a long and narrow (LN) channel; its length is 20 times its width.

The associated dynamical system is a rippled channel of infinite length. We use the top profile $y = \gamma + \nu\sin(2\pi x)$ as a surface of section to obtain Poincaré plots (x_n, p_n), where x_n (p_n) is the value of the x coordinate (momentum) right after the nth collision. Tennyson[14] has explored the dynamics of an approximate version of this map, which is valid for small values of ν/γ. The various types of dynamics are revealed in the Poincaré plots as we vary the value of ν. In Ref. 15 a complete panorama of the dynamics of this system is given. Figures 2(a) and 2(b) and Figs. 3(a) and 3(b) correspond to two dynamical regimes of LN and SW channels, respectively. We have chosen the common initial value of $x = 1/4$ in order to obtain all the possible types of trajectories allowed by the system even though the transmission quantities were calculated with an initial distribution Eq. (1) placed at $x = 0$.

The classical ballistic regime is realized at low temperatures in nanostructures where the size of the sample L is such that $\lambda_F \ll L \lesssim L_e$, where λ_F is the electron wavelength and L_e is the mean free path (see, e.g., the review in Ref. 7). Collisions with the boundaries in mesoscopic systems may alter considerably the distances traveled before exiting. To take this into account, the ballistic condition must require that L_e exceeds not only L but also the mean path length $\langle \lambda_t \rangle$. Numerical calculations of mean paths are therefore necessary in order to obtain an estimate for how large the device can be and still consider the motion as ballistic. Figures 4(a) and 5(a) plot the mean path lengths for the transmitted particles as a function of the ripple amplitude ν for LN and SW channels, respectively. Note that for both SW and LN channels, the mean path length approaches the value $\pi l/2$ (which can be obtained analytically[15]) as the channels become flat. Hence the mean path length is about 50% larger than the length l of the flat channel. The appearance of small ripples decreases the mean paths for both LN and SW channels, but the effect is more drastic for SW channels [see the
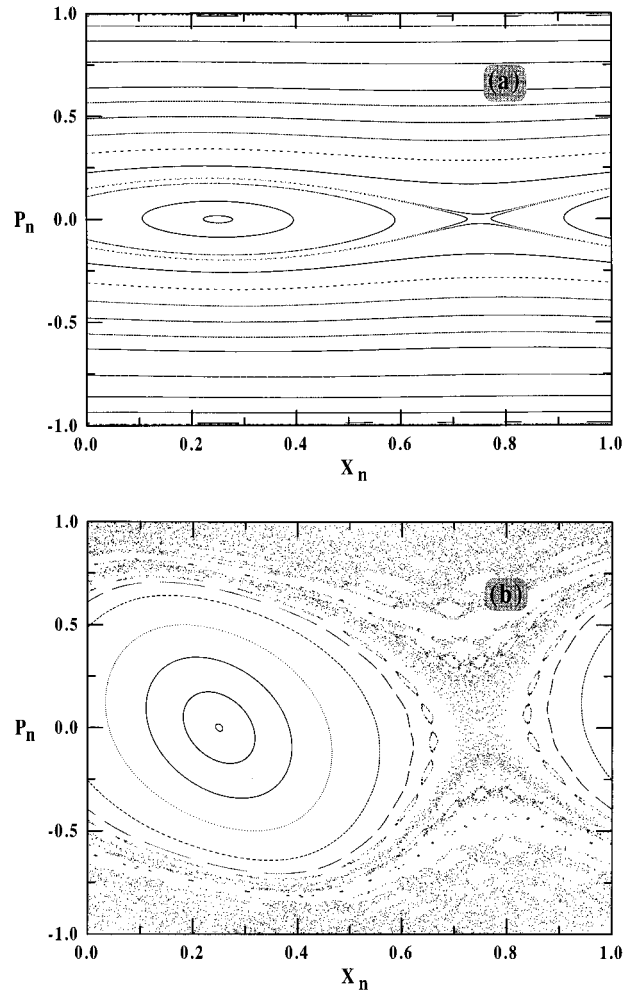

FIG. 2. Poincaré maps for electrons moving in the narrow channel ($\gamma = 0.1$). (a) $\nu = 0.001$ and (b) $\nu = 0.02$.

inset of Figs. 4(a) and 5]. For LN channels the mean path length does not exceed the flat channel value as long as the ripple is less than $\nu = 0.05$, which is half the channel's average width. $\langle \lambda_t \rangle$ increases substantially beyond this value. Throughout this steady increase the dynamics is qualitatively the same; all accessible orbits are chaotic, surrounding a large inaccessible resonance island.[15] In this dynamical regime the gradual decrease in $T(\nu)$ is simply due to the gradual increase of the boundary slope. For SW channels $\langle \lambda_t \rangle$ oscillates as ν increases but does not exceed the flat channel value except in the neighborhood of the peak at $\nu \simeq 0.9$. Thus, unless the ripples are very large the mean path length of the rippled channel is *shorter* than the flat channel value. Figures 4(b) and 5(b) plot the mean number of collisions of transmitted particles $\langle N_t(\nu) \rangle$ for LN and SW channels, respectively. The specularity parameter, the probability of specular reflection, can be as large as 0.9 (see, e.g., Ref. 16), which means that diffusive scattering is expected after about ten collisions. According to this criterion and to Figs. 4(b) and 5(b) there is no loss of memory for particles transmitted in SW channels and some diffusive scattering is expected for realistic LN channels. As regards the transmissivity $T(\nu)$, one would naturally expect it to decay as the amplitude of the ripple increases. Such is the case for the LN
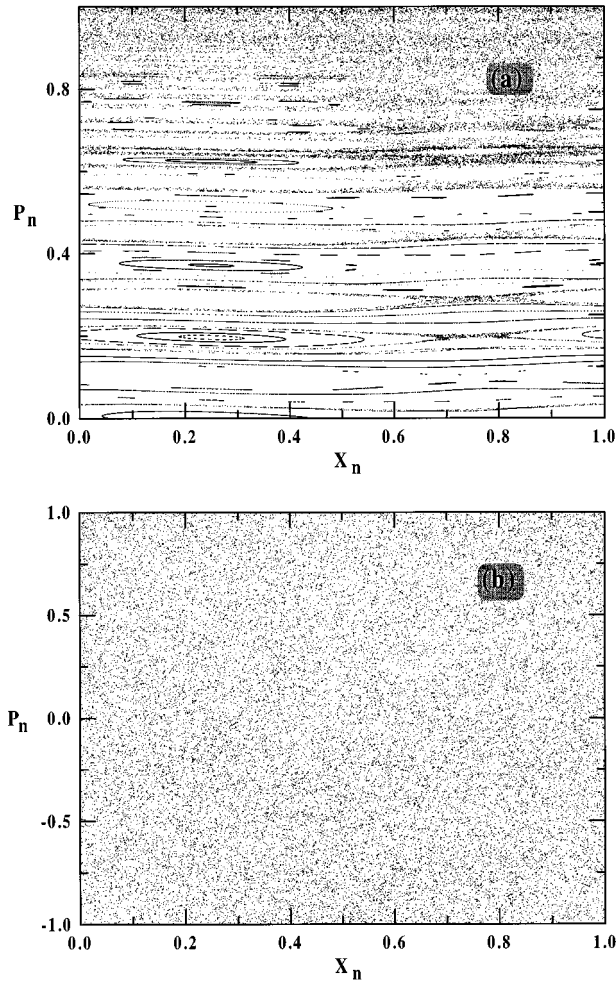
FIG. 3. Poincaré maps for electrons moving in the wide channel ($\gamma = 5.0$). (a) $\nu = 0.001$ and (b) $\nu = 0.01$. For symmetry and to show a more detailed map in case (a) we plot the p axis from 0 to 1.

channel [Fig. 4(c)] but for the SW channel, Fig. 5(c) shows that the decrease is not monotonic. In Sec III B we shall discuss the mechanism responsible for this behavior.

III. DYNAMICAL ORIGIN OF TRANSPORT PROPERTIES

The Poincaré plots were generated to reveal the various types of orbits produced by the dynamical system, while the transmission quantities were obtained by following the trajectories of each of the 10^5 particles injected at the left lead with a cosine distribution Eq. (1). Explicitly, this was accomplished by distributing homogeneously along the y axis 100 "sources." Each source injected 1000 particles (rays) with a cosine distribution.

A. Long and narrow channel

The 10^5 initial conditions corresponding to the injected particles would fall on the various types of "accessible" orbits in the Poincaré plots (x_n, p_n). Accessible orbits are those orbits in the Poincaré plots that can be reached from the initial conditions of the injected particles. One type of orbit *not* accessible are those ellipses [the first-order resonance islands centered at $x = 0.25$ in Figs. 2(a) and 2(b)] that
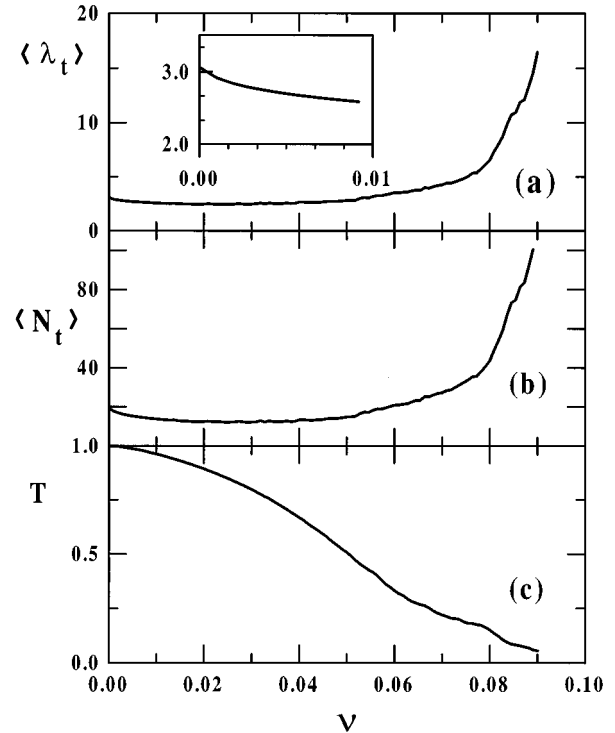

FIG. 4. Transport characteristics for the LN channel vs ripple amplitude: (a) dimensionless mean free path, (b) mean number of collisions for transmitted particles, and (c) transmissivity. The inset of (a) is a zoom of the mean path length near $\nu = 0$.

do not cross the p_n axis $x = 0$. They correspond to particles trapped within the widest part of the channel. Another example of nonaccessible orbits is the unstable, period-one orbit of the hyperbolic fixed point $(x_n, p_n) = (3/4, 0)$. This orbit corresponds to a particle bouncing up and down *exactly* at the narrowest part of the channel with *exactly* zero velocity in the x direction. Reversibility of motion implies that this orbit is unreachable, inaccessible from any initial condition of the injected particles.

For sufficiently small values of ν, e.g, $\nu = 0.001$, the Poincaré plots are one-dimensional pendulumlike [see Fig. 2(a)], hence the motion is regular. The elliptic orbits correspond to particles colliding almost perpendicularly with the walls in the neighborhood of the maximum width of the channel, i.e., about $x = 1/4$. They execute librational motion (similar to the pendulum's oscillations about the the stable equilibrium point), moving adiabatically forward and backward. For a certain initial angle α_0 at $x = 0$, the trajectory makes an angle β_0 (with the vertical) in the neighborhood of $x = 1/4$. As the particle moves forward in this librational mode, the angles β_n ($n = 1, 2, \dots$) decrease gradually until the particle reaches the turning point X_N, where $\beta_N \simeq 0$ [Fig. 1(b)]. For a given set of geometrical parameters there is a critical momentum $p_c = \sin(\beta_c)$ corresponding to the largest amplitude of librational motion at $x = 1/4$ [see Figs. 2(a) and 2(b)]. β_c can be estimated from the condition of adiabatic invariance

$$[\gamma + \nu \sin(2\pi x_n)]\cos(\beta_n) = [\gamma + \nu \sin(2\pi x_m)]\cos(\beta_m),$$
$$(2)$$

written for two arbitrary points (x_n, β_n) and (x_m, β_m). If we set $\beta_n = \beta_c$ and $\beta_m = \beta_N$, then $x_n = 1/4$ and $x_m = x_N$ is near
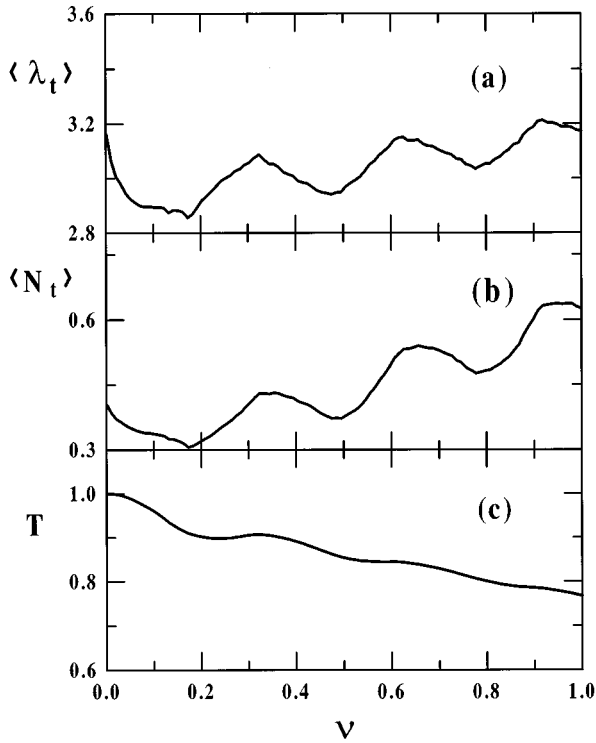
FIG. 5. Transport characteristics for the SW channel vs ripple amplitude: (a) dimensionless mean free path, (b) mean number of collisions for transmitted particles, and (c) transmissivity.

3/4. Substitution of these values into Eq. (2) gives, to the first order,

$$\beta_c \simeq (2\nu/\gamma)^{1/2}. \tag{3}$$

This parametric dependence of β_c gives also good estimates for the magnitude of β_c. The slightly wavy horizontal lines on Fig. 2(a) belong to particles translating slowly to the right ($p_n > 0$) or to the left ($p_n < 0$). The separatrix divides two types of motion: translational and librational. The appearance of the smallest ripple changes the topology of the phase space, allowing for the reflection of particles.

For perturbative values of ν, e.g., $\nu = 0.001$, the contribution to reflection comes only from initial conditions falling on the $p_n > 0$ plane in the accessible elliptical orbits. As ν increases in the range $0 < \nu \lesssim 0.01$ the accessible librational orbits occupy a larger region, hence the number of reflected particles increases, producing a monotonic decrease in $T(\nu)$. Initial conditions falling on the separatrix can also be reflected, but for this range of small values of ν the separatrix is so thin that its contribution to reflection is negligible.

As the ripple amplitude is further increased, the separatrix becomes chaotic with some sizable width [see Fig. 2(b)]. For this range of values of ν ($0.015 \lesssim \nu \lesssim 0.025$) reflection is due also to initial conditions on the chaotic separatrix. Numerical experiments show[15] that the particles on the separatrix dwell for a long time in the neighborhood of the hyperbolic fixed point $(x,p) = (0,3/4)$, which is an example of a chaotic repeller (see, e.g., Refs. 6, 17, and 18). Plots of the total number of collisions N_c as a function of initial angle α_0 reveal the fractal structure associated with these

repellers.[15] The fractality of such functions is usually taken as the signature of chaotic scattering.[17–19]

For the range $0.015 \lesssim \nu < 0.025$, the accessible chaotic region outside the chaotic separatrix (and with $p_n > 0$) does not contribute to reflection because Kolmogorov-Arnon'd-Moser (KAM) curves forbid its connection with the chaotic separatrix and with the chaotic region for negative p_n. There is a critical value of ν (≈ 0.025) for which the last KAM curve is destroyed and then all chaotic regions are connected. After this value of ν one would expect the transmission curve to decay faster since more and more initial conditions fall on the chaotic sea and hence the probability of being reflected increases sharply. This is not the case, as Fig. 4(c) shows. Poincaré plots in this range of ν indicate that there is a competing mechanism, namely, the number of librational orbits accessible to the initial conditions also decreases, and hence fewer particles are reflected by libration, as ν increases. Thus the slope of the curve $T(\nu)$ remains roughly constant during this change in the dynamics.

B. Short and wide channel

Here the most notorious feature is the nonmonotonic decay of $T(\nu)$ [Fig. 5(c)]. The motion of the associated dynamical system (the infinite channel) becomes chaotic even for small values of ν (see Fig. 3). However, the Poincaré plots provide no clue for understanding the nonmonotonic decay of $T(\nu)$ because the channel is so short and wide that the great majority of particles transmit with zero or one collision. Instead, we shall analyze the response function $N_t(\alpha_0)$, which is the number of collisions for a transmitted particle injected with initial angle α_0. For flat SW channels ($\nu = 0$) $N_t(\alpha_0)$ is a stepwise function (dashed line on Fig. 6) with two infinite maxima at $\alpha_0 = \pm 90°$ and a wide central transmission window with $N_t = 0$. For rippled SW channels, other peaks and secondary transmission windows appear (solid lines in Fig. 6). Figures 7(a)–7(c) plot $N_t(\alpha_0)$ in the region to the right of the central window for $\nu = 0.3183 \approx 1/\pi$, $\nu = 0.4775 \approx 1.5/\pi$, and $\nu = 0.6366 \approx 2/\pi$,
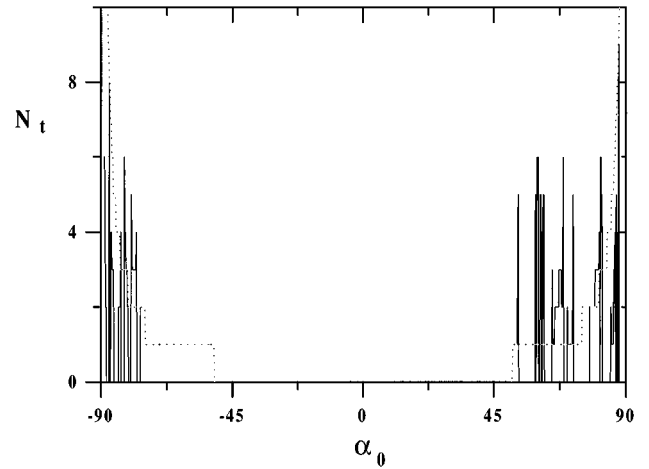

FIG. 6. Number of collisions $N_t(\alpha_0)$ for the particle transmitted through the SW channel ($\gamma = 5$) vs initial angle α_0. The solid and dashed lines are for the rippled ($\nu = 0.222$) and flat ($\nu = 0$) channels.
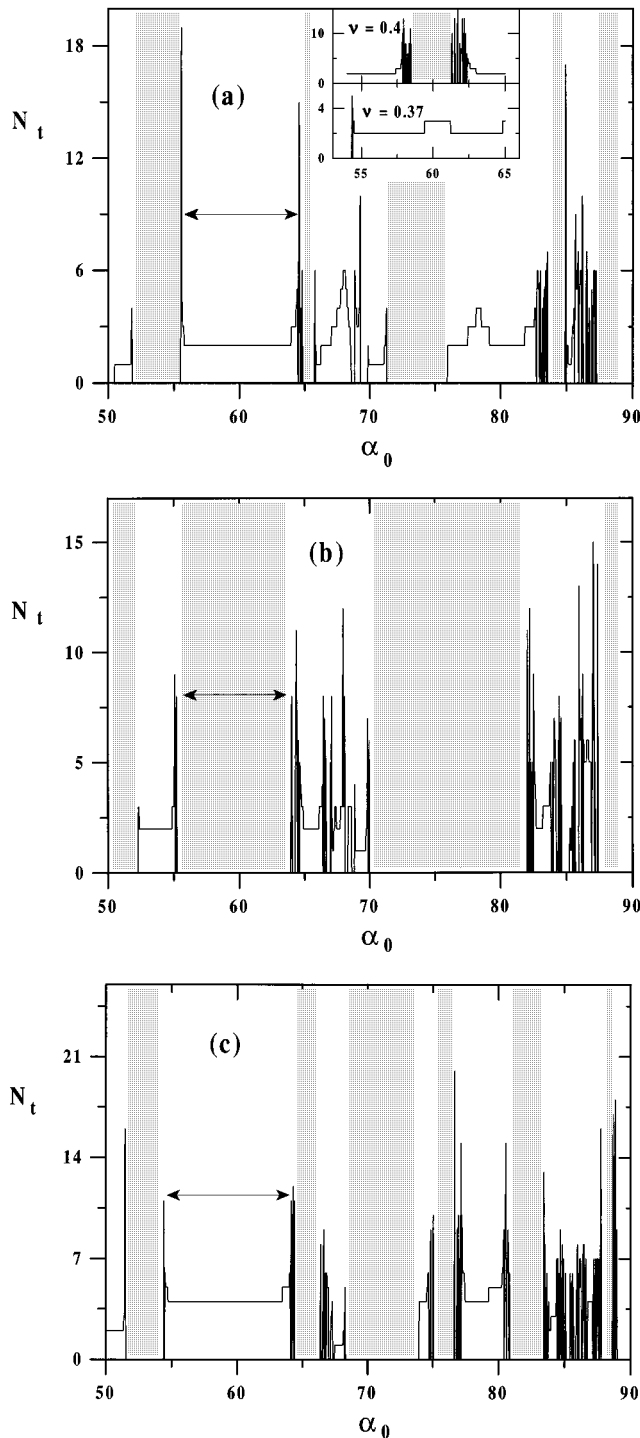
FIG. 7. Evolution of a secondary window of transmission (delimited by arrows) with the increase of the ripple amplitude. The shaded regions indicate intervals that correspond to the reflected particles. (a) $\nu=1/\pi$, the window is spreading; (b) $\nu=1.5/\pi$, the window is closed; (c) $\nu=2/\pi$, the window is opened again. Inset: fragmentation of the secondary window in the vicinity of its maximum.

respectively. These are the values for the first maximum, second minimum, and second maximum of $\langle T(\nu)\rangle$, respectively. The interval delimited by arrows in Fig. 7(a) is a secondary transmission window, born at around $\nu=0.235$, which is where $T(\nu)$ starts to level off after a steady de-

crease [Fig. 5(c)]. This interval is the largest secondary window and it continues to grow as ν increases, reaching a maximum width at around $\nu=0.37$. Beyond this value the transmission window breaks into smaller windows with a pattern shown in the inset in Fig. 7(a). As ν continues to increase, the secondary window continues to fragment, "pulverizing," until at around $\nu=0.4775\approx1.5/\pi$ the window is "closed" against the transmitted particles [see Fig. 7(b)]. This transmitted window appears again for $\nu>1.5/\pi$ and reaches its second maximum at $\nu=2/\pi$ [Fig. 7(c)]. Note also that at $\nu=1.5/\pi$ another wide region, forbidden for the transmitted particles, appears in the interval $70°<\alpha_0<82°$. These two forbidden regions provide the second minima of the transmissivity $T(\nu)$. In Figs. 7(a)–7(c) the forbidden regions are shaded. This pattern—the birth, growth, fragmentation, and disappearance of the transmission windows—oscillates with ν. Thus the overall decay of the transmission is due to the narrowing of the central transmission window whereas the nonmonotonic decay is due to the birth, growth, and destruction of the secondary transmission windows. These windows, intervals of measure one in the initial conditions, have been discussed previously by Roukes and Alerhand[8] and denoted as geometrical channels. Our results show that the existence of these geometrical channels has a noticeable effect on the transmissivity of short and wide channels.

IV. RANDOM VS DETERMINISTICALLY CHAOTIC SCATTERING

There is a one to one correspondence between the type of trajectories (regular or chaotic) observed in the Poincaré plots and the statistics of sequences of y values at the collision points. Specifically, power spectrum calculations of the effective profile give quasiperiodic function and broadband noise for regular and chaotic orbits, respectively.[15] Thus chaotic scattering on deterministic profiles is practically indistinguishable from scattering on a random profile. We now use this analogy to explain the parabolic decay of $T(\nu)$ obtained numerically for SW channels [see Fig. 8(a)]. It is well known (see, e.g., Ref. 20) that the classical resistivity ρ of a plate with rough surfaces increases quadratically, $\rho\propto\zeta^2/d^2$, with the rms height of roughness ζ. This expansion is valid for small ζ ($\zeta\ll d$) when the reflection from the rough boundary is almost specular. The resistance ρ of a channel is expressed through the transmissivity T by the well-known Landauer formula[21]

$$\rho\propto\frac{1-T}{T}. \qquad (4)$$

Since $T\rightarrow1$ as $\zeta\rightarrow0$, one obtains that

$$T(\zeta)=1-\kappa\zeta^2, \qquad (5)$$

where κ is a proportionality constant that depends on the geometry of the channel. Assuming that the rms height ζ of the roughness of the effective random profile is proportional to the amplitude of the ripples ν, we conclude that the parabolic dependence of $T(\nu)$ in the vicinity of $\nu=0$ is consistent with the chaotic character of the electron motion.
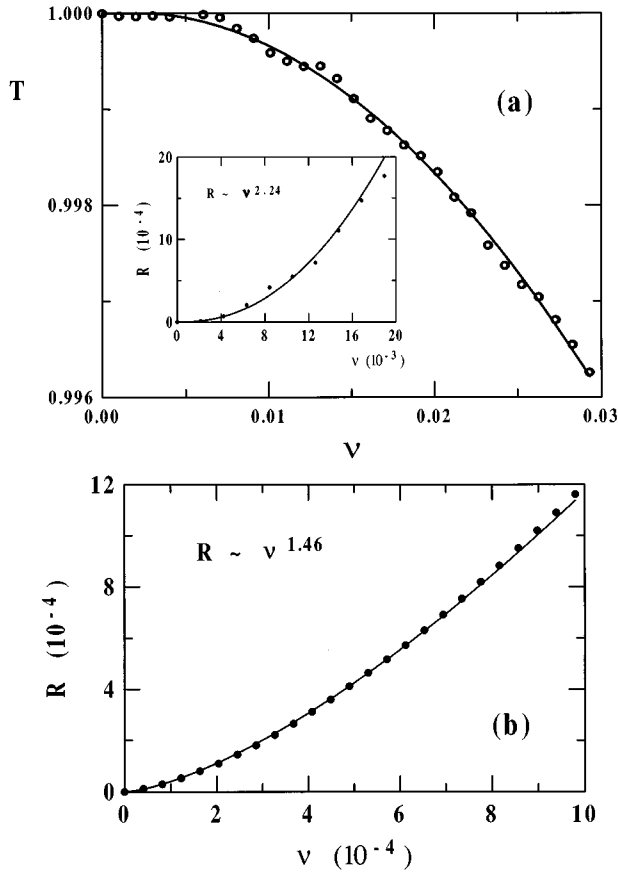
FIG. 8. (a) Transmissivity of the SW channel vs ripple amplitude. Inset: reflectivity vs ripple amplitude for 10^6 injected particles. (b) Reflectivity of the LN channel vs ripple amplitude for 10^6 injected particles.

In contrast, the dynamics is almost completely regular for LN channels even as the ripple amplitude increases to about $\nu = 0.015$. The phase space is dominated by KAM tori in a pendulumlike fashion and the analogy with scattering at the random boundary fails. The motion of electrons with angles $\alpha_0 \to \pi/2$ can be considered in the adiabatic approximation. The reflected electrons move almost perpendicularly to the boundaries with small longitudinal velocity $v_x \propto \cos\alpha_0 \approx \beta_0$ and produce a backward flux

$$R = 1 - T \simeq \frac{d}{n_0} \int_0^{\beta_c} \beta_0 \rho(\pi/2 - \beta_0) d\beta_0 \simeq \beta_c^3, \qquad (6)$$

which is proportional to $\nu^{3/2}$ [see Eq. (3)]. Thus the transmissivity of a channel with regular dynamics of particles decays faster than that for a channel with chaotic dynamics. In Figs. 8(a) (inset) and 8(b) we plot the reflectivity $R = 1 - T$ vs ν for the initial distribution of 10^6 particles.[22] The curve $R(\nu)$ for the SW channel fits the dependence $R(\nu) \sim \nu^{2.24}$ and that of the LN channel fits $R(\nu) \sim \nu^{1.46}$. Our analysis here predicts ν^2 (random) and $\nu^{1.5}$ (regular), respectively. For LN channels the agreement between analytical and numerical results is very good. The reason for the discrepancy

in SW channels is that the number of collisions in the SW channel is not large enough to provide a statistical average over the ensemble of effective random profiles. Numerical experiments with wide channels demonstrate that the exponent ϵ in ν^ϵ slowly approaches 2 as the length l of the channel increases.

An experimentally measurable quantity is the resistivity ρ of the channel. According to Eqs. (5) and (6), we conclude that ρ increases (in the region of small ν) proportionally to $\nu^{3/2}$ for regular and to ν^2 for chaotic dynamics of electrons in the channel. Qualitatively different behavior for the weak localization peak in the magnetoresistance of ballistic microstructures in the shape of a stadium and a circle has been observed recently in experiments[1,2] and explained theoretically.[23] Note that experiments[1,2] are concerned with a quantum effect (weak localization peak) in systems that are classically chaotic or regular. Here we propose a criterion that is related to the measurement of classical resistivity of a classical ballistic channel.

V. CONCLUSION

We have carried out classical calculations of transmission, mean path length, and mean number of collisions for an initial cosine distribution of 10^5 and 10^6 electrons injected into an electron conducting channel with a periodically modulated profile. Two distinct representative geometries were analyzed in detail, namely, short-wide channels and long-narrow channels. The curves for mean path lengths and mean number of collisions may be used to estimate the validity of the ballistic regime. The dynamical system exhibits the generic transition to chaos as the ripple amplitude (ν) increases. The contribution of the regular and chaotic regions to reflection and transmission was identified. The Poincaré plots were most useful for understanding transmission features for the LN channel essentially because the particles dwell, on the average, for a sufficiently long time.

The number of collisions as a function of initial angle $N_t(\alpha_0)$ proved to be a very useful response function for understanding features of the transmission curves for both narrow and wide channels. The curves for $N_t(\alpha_0)$ show windows of transmission and reflection in between high sharp peaks of reflection or transmission that depend strongly on the initial condition α_0 and possess fractal structure associated with the chaotic repellers of the system. The main contribution to the mean number of collisions and mean path length comes from initial conditions in these windows (or geomerical channels). The nonmonotonic decay of the transmission of particles in SW channels results from the birth, growth, and fractalization of secondary transmission windows.

Based on analytical and numerical calculations, we propose a criterion to distinguish between regular and chaotic dynamics of electrons in the rippled channel by measuring its classical resistivity ρ as a function of ripple amplitude ν. For the case of regular dynamics $\rho(\nu) \propto \nu^{3/2}$ and for the chaotic dynamics $\rho(\nu) \propto \nu^2$ in the region of small ν.

Finally, we remark that the quantum study of this system is of interest as a means of exploring the correspondence between classical and quantum transport and dynamical properties in both integrable and chaotic regimes.[13]

[1] A. M. Chang, H. U. Baranger, L. N. Pfeiffer, and K. W. West, Phys. Rev. Lett. **73**, 2111 (1994); H. U. Baranger, Physica D **83**, 30 (1995), and references therein.

[2] C. M. Marcus, A. J. Rimberg, R. M. Westervelt, P. F. Hopkins, and A. C. Gossard, Phys. Rev. Lett. **69**, 506 (1992).

[3] L. E. Reichl, *The Transition to Chaos in Conservative Classical Systems; Quantum Manifestations* (Springer-Verlag, New York, 1992); F. Haake, *Quantum Signatures of Chaos* (Springer-Verlag, Berlin, 1991); K. Nakamura, *Quantum Chaos: A New Paradigm of Nonlinear Dynamics* (Cambridge University Press, New York, 1994).

[4] Yu. Galperin and V. I. Kozub, Europhys. Lett. **15**, 631 (1991).

[5] V. I. Kozub and A. A. Krokhin, Zh. Éksp. Teor. Fiz. **101**, 1333 (1992) [Sov. Phys. JETP **74**, 715 (1992)]; J. Phys. Condens. Matter **5**, 9135 (1993).

[6] V. J. Kozub, Europhys. Lett. **18**, 337 (1992).

[7] C. W. Beenakker and H. van Houten, in *Solid State Physics: Advances in Research and Applications*, edited by H. Ehrenreich and D. Turnbull (Academic, New York, 1991), Vol. 44, pp. 1–228.

[8] M. L. Roukes and O. L. Alerhand, Phys. Rev. Lett. **65**, 1651 (1990).

[9] M. L. Roukes, A. Scherer, and B. P. Van der Gaag, Phys. Rev. Lett. **64**, 1154 (1990).

[10] K. L. Shepard, M. L. Roukes, and B. P. Van de Gaag, Phys. Rev. B **46**, 9648 (1992).

[11] C. W. J. Beenakker and H. van Houten, Phys. Rev. Lett. **63**, 1857 (1989).

[12] R. J. Blaikie, K. Nakazato, J. R. A. Cleaver, and H. Ahmed, Phys. Rev. B **46**, 9796 (1992).

[13] G. A. Luna-Acosta, K. Na, L. E. Reichl, and A. Krokhin, Phys. Rev. E **53**, 3271 (1996).

[14] J. L. Tennyson, in *Nonlinear Dynamics and the Beam-Beam Interaction*, edited by M. Month and J. C. Herrera, AIP Conf. Proc. No. 57 (AIP, New York, 1979), p. 158.

[15] G. A. Luna-Acosta, A. A. Krokhin, M. A. Rodríguez, and P. H. Hernández-Tejeda (unpublished).

[16] T. J. Thornton, M. L. Roukes, A. Scherer, and B. P. Van de Gaag, Phys. Rev. Lett. **63**, 2128 (1989).

[17] E. Ott, *Chaos in Dynamical Systems* (Cambridge University Press, New York, 1993).

[18] P. Gaspard, Chaos **3**, 427 (1993).

[19] B. Eckhardt, Physica D **33**, 89 (1988); Y. C. Lai and C. Grebogi, Int. J. Bifur. Chaos **1**, 667 (1991); R. Blumel and U. Smilansky, Phys. Rev. Lett. **60**, 477 (1988); A. Zacherl, T. Geisel, J. Nierwetberg, and G. Radons, Phys. Lett. **114A**, 317 (1986).

[20] A. V. Chaplic and M. V. Éntin, Zh. Éksp. Teor. Fiz. **55**, 990 (1968) [Sov. Phys. JETP **28**, 514 (1969)]; Z. Tešanovic, M. V. Jaric, and S. Maekava, Phys. Rev. Lett. **57**, 2760 (1986); N. Trivedi and N. Ashcroft, Phys. Rev. B **38**, 12 298 (1988); Chr. Kunze, Solid State Commun. **87**, 359 (1993); R. Link and A. Knäbchen, J. Phys. Condens. Matter **5**, 6563 (1993); A. E. Meyerovich and S. Stepaniants, Phys. Rev. Lett. **73**, 316 (1994); A. E. Meyerovich and S. Stepaniants, Phys. Rev. B **51**, 17 116 (1995).

[21] R. Landauer, IBM J. Res. Dev. **1**, 233 (1957).

[22] These numerical experiments require a larger number of injected particles to eliminate some of the coarse graining in $T(\nu)$ [Fig. 8(a)] produced by the discrete distribution of injected particles.

[23] W. A. Lin, J. B. Delos, and R. V. Jensen, Chaos **3**, 665 (1993).